Article:
Buksa, H., Johnson, E.C. orcid.org/0000-0002-0092-1008, Chan, D.H.H. et al. (4 more authors) (2024) Arginine-functional methacrylic block copolymer nanoparticles: synthesis, characterization, and adsorption onto a model planar substrate. Biomacromolecules, 25 (5). pp. 2990-3000. ISSN 1525-7797

https://doi.org/10.1021/acs.biomac.4c00128

Biomacromolecules

Open Access

pubs.acs.org/Biomac

Article

Arginine-Functional Methacrylic Block Copolymer Nanoparticles: Synthesis, Characterization, and Adsorption onto a Model Planar Substrate

Published as part of Biomacromolecules virtual special issue "Fundamentals of Polymer Colloids".

Hubert Buksa, Edwin C. Johnson, Derek H. H. Chan, Rory J. McBride, George Sanderson, Rebecca M. Corrigan, and Steven P. Armes*

Cite This: *Biomacromolecules* 2024, 25, 2990−3000

Read Online

ACCESS | Metrics & More | Article Recommendations | Supporting Information

ABSTRACT: Recently, we reported the synthesis of a hydrophilic aldehyde-functional methacrylic polymer (*Angew. Chem.*, **2021**, *60*, 12032−12037). Herein we demonstrate that such polymers can be reacted with arginine in aqueous solution to produce arginine-functional methacrylic polymers without recourse to protecting group chemistry. Careful control of the solution pH is essential to ensure regioselective imine bond formation; subsequent reductive amination leads to a hydrolytically stable amide linkage. This new protocol was used to prepare a series of arginine-functionalized diblock copolymer nanoparticles of varying size via polymerization-induced self-assembly in aqueous media. Adsorption of these cationic nanoparticles onto silica was monitored using a quartz crystal microbalance. Strong electrostatic adsorption occurred at pH 7 (Γ = 14.7 mg m^{-2}), whereas much weaker adsorption occurred at pH 3 (Γ = 1.9 mg m^{-2}). These findings were corroborated by electron microscopy, which indicated a surface coverage of 42% at pH 7 but only 5% at pH 3.

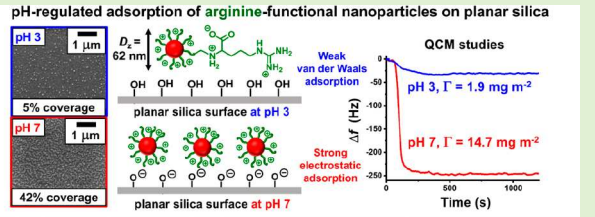

INTRODUCTION

Recently, there has been increasing interest in synthetic polymers bearing arginine moieties owing to their potential bioapplications. Arginine-functionalized polymers have been examined as a platform technology for (i) gene or drug delivery and (ii) antimicrobial coatings.[1−4] More specifically, arginine polymers have been synthesized via Michael-type polyaddition, polycondensation, or radical cross-linking of poly(arginine methacrylate) for use as cell-permeating peptides, polyamide transfection agents, or antimicrobial hydrogels, respectively.[5−7] In view of the development of multidrug-resistant pathogens such as *Staphylococcus aureus* and *Pseudomonas aeruginosa*,[8] there has been a concerted effort to prepare new antimicrobial polymers via reversible addition−fragmentation chain transfer (RAFT) polymerization of arginine-mimicking monomers. For example, Xu et al. grew antimicrobial arginine polymer brushes from planar substrates via surface-initiated RAFT polymerization while Perrier and co-workers designed antibacterial diblock copolymers and antifouling star copolymers using arginine-based acrylamides.[4,9,10] Unfortunately, the requirement for Boc or Fmoc protecting groups and the use of toxic organic solvents such as dichloromethane or dioxane significantly reduces the atom economy and cost-effectiveness of many of the above monomer syntheses. In principle, arginine conjugation to aldehyde-functionalized monomers via imine bond formation offers an attractive alternative route to arginine-functionalized polymers. However, until recently, all suitable aldehyde-functional vinyl monomers have been hydrophobic (e.g., 4-vinylbenzaldehyde) so their statistical copolymerization with a suitable hydrophilic vinyl monomer has been required to produce the desired water-soluble polymer.[11,12] This approach necessarily limits the degree of aldehyde functionality that can be incorporated into such copolymers.

Over the past decade or so, polymerization-induced self-assembly (PISA) has become an established platform technology for the efficient synthesis of a wide range of block copolymer nano-objects. Many examples of PISA reported in the literature involve RAFT polymerization,[13−29] and this radical-based chemistry is well-suited for the development of aqueous formulations.[30−45] For such syntheses, a water-soluble precursor is first prepared via RAFT solution polymerization and then chain-extended using a suitable vinyl monomer to produce an amphiphilic diblock copolymer. Once a critical degree of polymerization (DP) is achieved, the growing second block becomes insoluble and in

Received: January 30, 2024
Revised: April 16, 2024
Accepted: April 17, 2024
Published: May 2, 2024

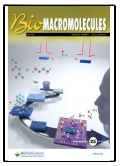

https://doi.org/10.1021/acs.biomac.4c00128
Biomacromolecules 2024, 25, 2990−3000

situ self-assembly occurs to produce nascent diblock copolymer nanoparticles. Depending on the reaction conditions, the initial spherical morphology is either retained or an evolution in morphology occurs to generate highly anisotropic worms, polydisperse vesicles or, in certain cases, lamellae.[46−50] RAFT polymerization is applicable to many functional vinyl monomers, which has enabled the rational design of a broad range of nanoparticles for various potential applications.[51−56]

Recently, we reported a new synthetic route to controlled-structure poly(amino acid methacrylates).[57] First, RAFT solution polymerization of a *cis*-diol-functional methacrylic monomer GEO5MA using a suitable dithiobenzoate RAFT agent produced a well-defined PGEO5MA homopolymer (M_w/M_n < 1.20). Subsequently, selective oxidation of the *cis*-diol groups using $NaIO_4$ was conducted in aqueous solution to produce an aldehyde-functional water-soluble precursor, followed by (i) reaction with various amino acids (e.g., glycine, lysine, or cysteine) and (ii) reductive amination to afford the desired poly(amino acid methacrylate). This approach was then extended to include various examples of histidine-functionalized diblock copolymer nano-objects prepared via aqueous PISA[58,59] and polymer brushes[60] prepared via atom transfer radical polymerization.[61]

Herein we exploit the above synthetic strategy to prepare a series of arginine-functionalized diblock copolymer nanoparticles (see Scheme 1). First, GEO5MA is used to prepare a water-soluble PGEO5MA precursor prior to RAFT aqueous dispersion polymerization of benzyl methacrylate to produce sterically stabilized spherical nanoparticles (see Scheme 2). These *cis*-diol-bearing nanoparticles are then reacted with arginine via Schiff base chemistry, followed by reductive amination using $NaCNBH_3$. In principle, arginine addition can occur via the primary amine of the amino acid or via the guanidine moiety to produce a binary mixture of isomers. However, we demonstrate that judicious selection of the solution pH ensures regioselectivity during imine bond formation, thus avoiding the protecting group strategy typically employed by others.[1,2,9,10] The quartz crystal microbalance (QCM) is a well-established surface analytical technique that has been used to study the adsorption of either inorganic or organic particles (including microorganisms) onto various planar substrates, including stainless steel and silica.[54,62−65] Accordingly, the physical adsorption of such arginine-functionalized nanoparticles on a model planar substrate is examined using QCM in combination with scanning electron microscopy (SEM). In principle, the arginine-functionalized nanoparticles depicted in Scheme 2 constitute an interesting model system for understanding the pH-modulated adsorption of soft nanoparticles onto a hard planar substrate.

EXPERIMENTAL SECTION

Materials. All chemicals were used as received, unless stated otherwise. GEO5MA monomer was kindly donated by GEO Specialty Chemicals (Hythe, UK). 2-Cyano-2-propyl dithiobenzoate (CPDB, > 97%), benzyl methacrylate (BzMA; 96%), 4,4′-azobis(4-cyanopentanoic acid) (ACVA; > 98%), sodium periodate ($NaIO_4$, ≥ 99.8%), sodium cyanoborohydride ($NaCNBH_3$, 95%), *L*-arginine (≥99.5%), and D_2O were purchased from Sigma-Aldrich (Gillingham, UK). d_6-Dimethyl sulfoxide (d_6-DMSO) was purchased from Goss Scientific Instruments Ltd. (Cheshire, UK). Dimethylformamide (DMF, ≥ 99.5%) and ethanol (≥99.5%) were purchased from Fisher Scientific (Loughborough, UK). Deionized water was obtained from an Elga Medica DV25 water purification setup.

Scheme 1. Synthesis of $PGEO5MA_{64}$ via RAFT Solution Polymerization of GEO5MA, Followed by Its Selective Oxidation Using $NaIO_4$ in Aqueous Media to Produce the Corresponding Aldehyde-Functional Polymer ($PAGEO5MA_{64}$)[a]

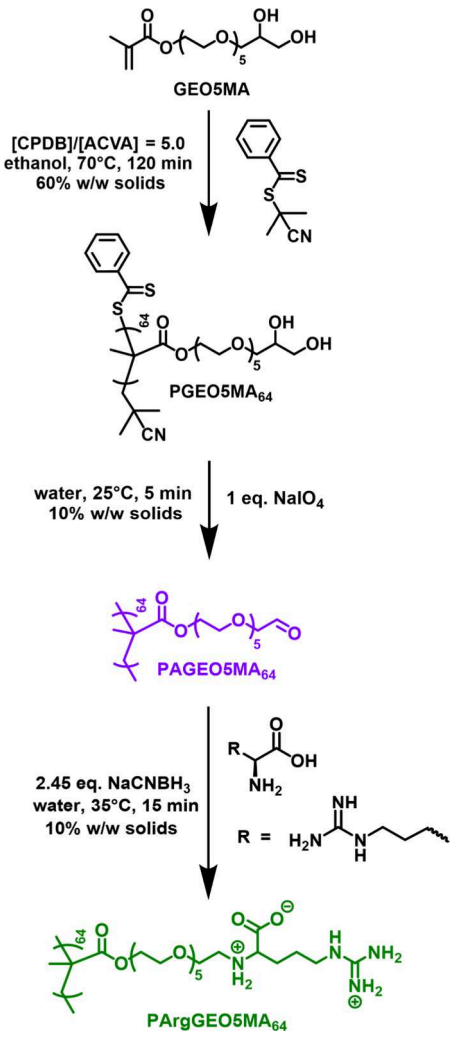

[a]Subsequent arginine functionalization at pH 10 produces the target $PArgGEO5MA_{64}$ homopolymer with regioselective control.

Methods. *^{1}H NMR Spectroscopy.* Spectra were recorded in either D_2O or d_6-DMSO using a 400 MHz Bruker Avance-400 spectrometer at 298 K with 16 scans being averaged per spectrum.

Gel Permeation Chromatography. Aqueous gel permeation chromatography (GPC) was used to determine the number-average molecular weights (M_n) and dispersities (M_w/M_n) for $PGEO5MA_{64}$, $PAGEO5MA_{64}$, and $PArgGEO5MA_{64}$ homopolymers. These polymers were analyzed at 1% w/w using an aqueous buffer eluent containing 0.1 M $NaNO_3$, 0.02 M triethylamine, 0.05 M $NaHCO_3$, and 0.03% NaN_3 adjusted to pH 10.0 using 1.0 M NaOH. The GPC setup comprised an Agilent 1260 Infinity instrument equipped with a degasser, pump, a guard column, three columns connected in series (PL-Aquagel Mixed-H, OH-30, and OH-40), and a refractive index detector. The column and detector temperature was set at 35 °C, and the flow rate was 1.0 mL min^{-1}. Calibration was achieved using a series of nine near-monodisperse poly(ethylene oxide) standards ranging from 2.1 to 969 kg mol^{-1}, and data were analyzed using Agilent GPC/SEC software.

DMF GPC was used to characterize the $PGEO5MA_{64}$ homopolymer and all diblock copolymers. These samples were analyzed at 1.0% w/w using HPLC-grade DMF eluent containing 10 mmol LiBr

https://doi.org/10.1021/acs.biomac.4c00128
Biomacromolecules 2024, 25, 2990−3000

Scheme 2. Synthesis of PGEO5MA$_{64}$−PBzMA$_x$ Nanoparticles via RAFT Aqueous Emulsion Polymerization of Benzyl Methacrylate at 70°C[a]

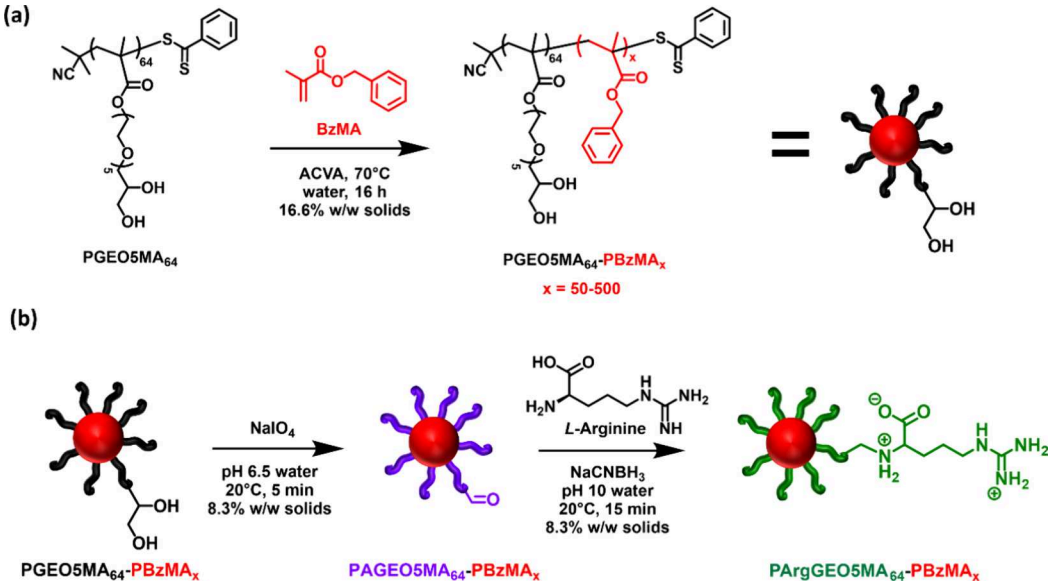

[a]The resulting *cis*-diol functional nanoparticles are first oxidized using $NaIO_4$ and then reacted with arginine via Schiff base chemistry, and the subsequent reductive amination using $NaCNBH_3$ affords the target arginine-functional nanoparticles.

(Figure S1). The GPC setup comprised an Agilent 1260 Infinity instrument equipped with a degasser, pump, a guard column, two PL-gel 5 μm Mixed-C columns connected in series, and a refractive index detector. Calibration was achieved using a series of 11 near-monodisperse poly(methyl methacrylate) standards ranging from 2.38 to 2200 kg mol^{-1}, and data were analyzed using Agilent GPC/SEC software.

Dynamic Light Scattering. Dynamic light scattering (DLS) studies were performed using a Malvern Zetasizer Nano-ZS instrument equipped with a 4 mW He−Ne laser (λ = 633 nm) operating at a fixed scattering angle of 173°. Copolymer dispersions were diluted to 0.1% w/w using deionized water prior to light scattering studies at 25 °C, with 2 min being allowed for thermal equilibrium prior to each measurement. The hydrodynamic *z*-average particle diameter was calculated via the Stokes−Einstein equation, which assumes perfectly monodisperse, noninteracting spheres. The polydispersity index is expressed as a standard deviation that indicates the breadth of the particle size distribution, rather than the experimental error.

Aqueous Electrophoresis. Zeta potentials were determined using a Malvern Zetasizer Nano ZS instrument equipped with a 4 mW He−Ne laser (λ = 633 nm) operating at a fixed scattering angle of 173°. Diblock copolymer nanoparticle dispersions were diluted to 0.1% w/w with 1 mM KCl as background electrolyte using either dilute HCl or NaOH for pH adjustment as required. Zeta potentials (averaged over three consecutive runs) were calculated via the Henry equation using the Smoluchowski approximation.

Transmission Electron Microscopy. Copper/palladium transmission electron microscopy (TEM) grids (Agar Scientific, UK) were coated in-house to yield a thin film of amorphous carbon and were subjected to a glow discharge for 20 s. An aqueous droplet of a copolymer dispersion (7.0 μL, 0.1% w/w) was placed on freshly treated grids for 1 min and then carefully blotted with filter paper to remove excess solution. An aqueous droplet of uranyl formate solution (5.0 μL, 0.75% w/w) was placed on each sample-loaded grid for 1 min and then blotted with filter paper to remove excess stain. This negative staining protocol was required to ensure sufficient electron contrast. Each grid was then carefully dried using a vacuum hose. Imaging was performed at 80 kV using an FEI Tecnai Spirit 2 microscope fitted with an Orius SC1000B camera. Mean nanoparticle diameters were estimated by digital image analysis using *ImageJ* software.

QCM Studies. QCM sensors coated with a 50 nm silica overlayer (QSX 303, ~5 MHz fundamental frequency) were purchased from Biolin Scientific (Gothenburg, Sweden). Each sensor was cleaned according to the manufacturer's instructions. This four-step protocol involved (i) UV/O_3 treatment for 25 min (Bioforce UV/O_3 cleaner, 9 mW cm^{-2}, λ = 254 nm), (ii) exposure to 2% w/w sodium dodecyl sulfate solution for 30 min, (iii) rinsing with deionized water (iv), drying using a stream of N_2 gas, and (v) a final UV/O_3 treatment for 25 min. QCM measurements were performed using an openQCM NEXT instrument (Novatech Srl., Italy) equipped with a temperature-controlled cell connected to a Masterflex Digital Miniflex peristaltic pump (Cole-Parmer Instrument Co Ltd., St Neots, UK). The cleaned substrates were initially equilibrated with deionized water, then exposed to an aqueous dispersion of 1.0% w/w nanoparticles, and finally washed with deionized water to remove any weakly adhering nanoparticles. Measurements were performed at 25 °C using a flow rate of 0.10 mL min^{-1}. The mass of adsorbed nanoparticles was calculated using the Sauerbrey equation, which assumes the formation of a rigid thin film and relates the change in resonant frequency (Hz), Δf, to the change in adsorbed mass per unit area, Δm, via a sensitivity constant C (where C = −0.177 mg m^{-2} Hz^{-1}) and the harmonic number n.

$$\Delta m = C \times \frac{\Delta f}{n} \tag{1}$$

For the present study, the third harmonic (n = 3) was selected to calculate the adsorbed amount (expressed in mg m^{-2} and denoted as Γ) in order to avoid experimental artifacts associated with the fundamental harmonic that can occur if the sample mounting on the sensor is imperfect.[66−68]

Scanning Electron Microscopy. After nanoparticle adsorption experiments, selected silica-coated QCM sensors were sputter-coated with a 5 nm layer of gold and SEM images were captured using an Inspect-F instrument operating at an accelerating voltage of 10 kV and a beam current of 200 nA.

Synthetic Protocols. *Synthesis of the PGEO5MA$_{64}$ Precursor via RAFT Solution Polymerization in Ethanol.* GEO5MA monomer (30.0 g, 0.079 mol), CPDB (0.146 g, 0.66 mmol), ACVA initiator (0.037 g, 0.132 mmol; CPDB/ACVA molar ratio = 5.0), and ethanol (20.0 g) were weighed into a 50-mL round-bottomed flask. This reaction mixture was degassed with N_2 for 30 min, and the flask was

https://doi.org/10.1021/acs.biomac.4c00128
Biomacromolecules 2024, 25, 2990−3000

placed in an oil bath set at 70 °C for 120 min. The polymerization was quenched by removing the flask from the oil bath and exposing its contents to air while cooling to 20 °C. ^{1}H NMR studies confirmed the GEO5MA conversion to be 53% as judged by the attenuation of the GEO5MA vinyl protons at 5.7−6.1 ppm to the overlapping PGEO5MA and GEO5MA monomer oxymethylene proton signals at 4.1 and 4.3 ppm, respectively. Crude PGEO5MA was purified by precipitation into excess diethyl ether. The precipitate was redissolved in methanol, and the precipitation step was repeated. The PGEO5MA product was redissolved in deionized water, dialyzed for 2 days (with three changes of water per day), and then freeze-dried overnight to produce a red viscous liquid. The mean DP of the purified PGEO5MA precursor was estimated to be 64 via end-group analysis using ^{1}H NMR spectroscopy (the integrated aromatic protons assigned to the phenyl end-group derived from the RAFT agent at 7.3−8.0 ppm were compared to the integrated methacrylic backbone protons at 0.80−2.30 ppm).

Oxidation of PGEO5MA$_{64}$ Homopolymer Using NaIO$_4$. PGEO5MA$_{64}$ homopolymer (0.30 g, 12.2 μmol) and 0.70 g of deionized water were weighed into a 15-mL vial and stirred to produce an aqueous solution. Then an aqueous solution of 0.39 M $NaIO_4$ (2.0 mL) was added, and the reaction mixture was stirred for 5 min at 25 °C. A $NaIO_4$/GEO5MA molar ratio of unity was targeted to ensure full oxidation of the pendent *cis*-diol groups. The degree of oxidation was estimated using ^{1}H NMR spectroscopy by comparing the integrated proton signal adjacent to the geminal diol group at 5.1 ppm to that of the oxymethylene proton signal at 4.1 ppm. The resulting 10% w/w aqueous solution of PAGEO5MA was dialyzed against deionized water for two days (with three changes of water per day).

Reductive Amination of PAGEO5MA$_{64}$ Homopolymer Using Arginine and NaCNBH$_3$. *L*-Arginine (49.5 mg, 0.285 mmol) was dissolved in a 10% w/w aqueous solution of PAGEO5MA$_{64}$ homopolymer (1.00 g), and the resulting solution was adjusted to either pH 6 (using 0.1 M HCl) or pH 10 (using 0.1 M NaOH). Then $NaCNBH_3$ (43.8 mg, 0.698 mmol) was added, and the reaction mixture was stirred at 35 °C for 15 min before being dialyzed against deionized water for 2 days (with three changes of water per day) to remove impurities and any unreacted reagents. The degree of arginine functionalization was estimated by using ^{1}H NMR spectroscopy to monitor the disappearance of the geminal diol proton signal at 5.1 ppm relative to the methacrylic backbone proton signals at 0.8−2.3 ppm. The selectivity of this derivatization was estimated by comparing the $-CH_2-C\underline{H}_2-NH-$ signal intensity at 3.1 ppm from the two aza-methylene protons associated with the amino acid group (see signal *c* in Figure 2) to that at 3.2 ppm from the two aza-methylene protons associated with the guanidine group (see signal *d* in Figure 2).

Synthesis of PGEO5MA$_{64}$−PBzMA$_x$ Nanoparticles via RAFT Aqueous Emulsion Polymerization of Benzyl Methacrylate. The following synthesis of PGEO5MA$_{64}$−PBzMA$_{500}$ nanoparticles at 16.6% w/w solids is representative of the general protocol. BzMA monomer (0.31 g, 1.76 mmol), PGEO5MA$_{64}$ precursor (0.086 g, 3.5 μmol; target PBzMA DP = 500), ACVA initiator (0.30 mg, 1.2 μmol; PGEO5MA$_{64}$/ACVA molar ratio = 5.0), and water (2.0 g; targeting 16.6% w/w solids) were weighed into a 15 mL glass vial. The mixture was purged with N_2 for 15 min, and the vial was placed in an oil bath at 70 °C. After 16 h, the BzMA polymerization was quenched by removing the vial from the bath and exposing the resulting aqueous dispersion to air while cooling to 20 °C. The final BzMA conversion was determined to be more than 99% via ^{1}H NMR spectroscopy by monitoring the reduction in intensity of the vinyl proton signals at 5.6−6.2 ppm relative to that of the methacrylic backbone signals at 0.80−2.30 ppm (Figure S2).

Selective Oxidation of PGEO5MA$_{64}$−PBzMA$_{500}$ Nanoparticles Using NaIO$_4$. Oxidation of PGEO5MA$_{64}$−PBzMA$_{500}$ nanoparticles at 8.3% w/w solids was conducted by adding 1.00 g of an aqueous solution of 0.10 M $NaIO_4$ to a 15 mL glass vial containing 1.00 g of a 16.6% w/w aqueous dispersion of PGEO5MA$_{64}$−PBzMA$_{500}$ nanoparticles (0.166 g, 1.47 μmol); the resulting reaction mixture was stirred for 5 min at 25 °C. A $NaIO_4$/GEO5MA molar ratio of unity was employed to target full oxidation of the pendent *cis*-diol groups. The mean degree of oxidation was estimated using ^{1}H NMR spectroscopy in d_6-DMSO (Figure S3). The resulting 8.3% w/w aqueous dispersion of PAGEO5MA$_{64}$−PBzMA$_{500}$ nanoparticles was dialyzed against deionized water for 2 days (with three changes of water per day).

Reductive Amination of PAGEO5MA$_{64}$−PBzMA$_x$ Nanoparticles Using Arginine and NaCNBH$_3$. The following reductive amination of PAGEO5MA$_{64}$−PBzMA$_{500}$ nanoparticles is representative of the general protocol. *L*-Arginine (8.36 mg, 48.0 μmol; arginine/aldehyde molar ratio = 1.0) was added to a 15 mL glass vial containing 1.00 g of an 8.3% w/w aqueous dispersion of PAGEO5MA$_{64}$−PBzMA$_{500}$ nanoparticles (0.083 g, 0.75 μmol), which was adjusted to pH 10 using 0.1 M NaOH. Excess $NaCNBH_3$ (7.39 mg, 118 μmol; 2.45 mol excess) was added, and this reaction mixture was stirred for 15 min at 35 °C. Unfortunately, PArgGEO5MA$_{64}$−PBzMA$_{500}$ proved to be insoluble in common NMR solvents (e.g., d_6-DMSO, CD_3OD, d_5-pyridine), which precluded analysis using this spectroscopic technique. The resulting 8.3% w/w aqueous dispersion of PArgGEO5MA$_{64}$−PBzMA$_{500}$ nanoparticles was dialyzed against deionized water for 2 days (with three changes of water per day).

RESULTS AND DISCUSSION

Synthesis of an Arginine-Functionalized Water-Soluble Homopolymer. We have recently reported the synthesis of the PGEO5MA precursor and its corresponding hydrophilic aldehyde-functional polymer (PAGEO5MA$_{64}$), elsewhere.[57] In principle, PAGEO5MA$_{64}$ can be derivatized with various amine-functionalized molecules (e.g., amino acids, oligopeptides, proteins or dyes).[57−59] For example, using arginine should yield an arginine-functionalized polymer, PArgGEO5MA. However, in our initial experiments, we found that reductive amination of PAGEO5MA using arginine at pH 6 yielded a binary mixture of isomers owing to a lack of regioselectivity under such conditions. More specifically, the desired major isomer (arginine attached via the *N*-terminus, see Figure 1) comprised only 79% of the isomeric mixture.

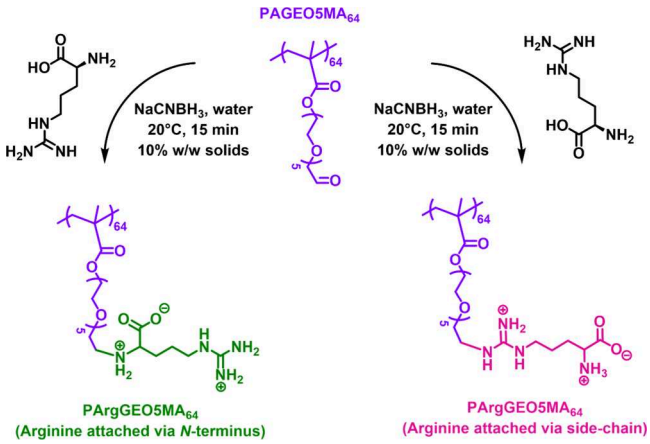

Figure 1. Schematic cartoon depicting the two possible isomers that may be formed when reacting PAGEO5MA$_{64}$ with arginine in the presence of $NaCNBH_3$.

This problem arises because both the primary amine and guanidine groups in arginine are protonated at pH 6. Hence, there is insufficient difference between these two potential reactive sites to ensure selectivity.

Fortunately, the primary amine group within arginine (pK_a 9.0) exists mainly in its neutral (nonprotonated) form at pH 10, while the guanidine group (pK_a 13.8) should remain in its

https://doi.org/10.1021/acs.biomac.4c00128
Biomacromolecules 2024, 25, 2990−3000

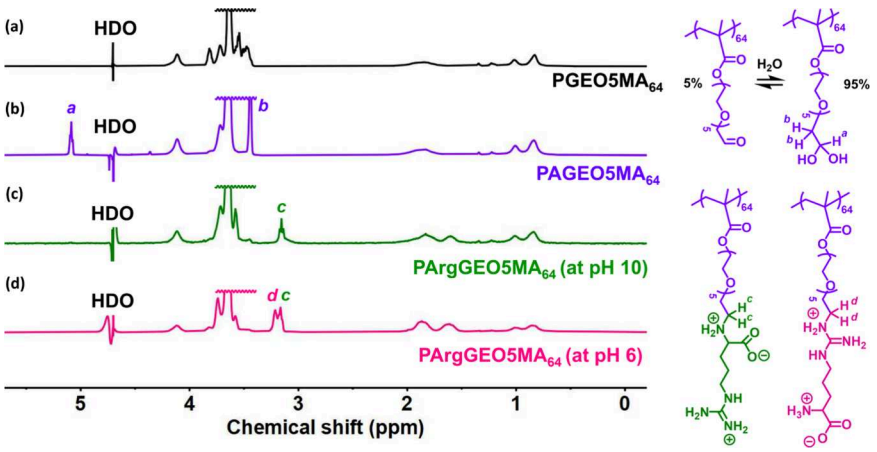

Figure 2. Effect of solution pH on regioselectivity. Partial ^{1}H NMR spectra recorded in D_2O (pH 6; using solvent suppression) for each step during the synthesis of PArgGEO5MA$_{64}$: (a) *cis*-diol functional PGEO5MA$_{64}$ precursor; (b) aldehyde-functional PAGEO5MA$_{64}$; (c) PArgGEO5MA$_{64}$ produced via reductive amination with arginine at pH 10 (regioselectivity under such conditions yields a single isomer); (d) binary mixture of PArgGEO5MA$_{64}$ products obtained via reductive amination with arginine at pH 6 (in this case, poor regioselective control produces two isomers).

protonated form under such conditions.[69] In principle, this should be sufficient to achieve the desired selectivity. Accordingly, the reductive amination of PAGEO5MA$_{64}$ using arginine was performed at pH 6 and pH 10, and the product(s) of these reactions were analyzed by ^{1}H NMR spectroscopy (Figure 2). Periodate oxidation of the PGEO5MA$_{64}$ precursor to form PAGEO5MA$_{64}$ produced two new proton signals associated with the geminal diol group, which is the hydrated form of aldehyde that is obtained in water (Figure 2b). Importantly, reductive amination of PAGEO5MA$_{64}$ with arginine at pH 10 yielded a single product (Figure 2c), as opposed to the binary mixture of isomers obtained at pH 6 (Figure 2d). Clearly, reductive amination of PAGEO5MA$_{64}$ with arginine at pH 10 provides a highly convenient wholly aqueous route to well-defined arginine-functionalized polymers.

Aqueous GPC was used to characterize the PGEO5MA$_{64}$ precursor, the aldehyde-functionalized PAGEO5MA$_{64}$, and the arginine-functionalized PArgGEO5MA$_{64}$ (Figure 3). Oxidation of PGEO5MA$_{64}$ to PAGEO5MA$_{64}$ involves the loss of formaldehyde, which results in a discernible reduction in M_n from 9.9 to 8.1 kg mol^{-1}. As expected, functionalization of PAGEO5MA$_{64}$ with arginine results in a significantly higher M_n for PArgGEO5MA$_{64}$. Moreover, the molecular weight distributions obtained for all three polymers are relatively narrow (M_w/M_n = 1.21−1.25), which indicates that each homopolymer is well-defined and that no side-reactions (e.g., branching or cross-linking) occurred during either oxidation or reductive amination.

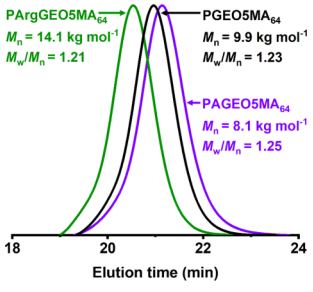

Figure 3. Aqueous GPC curves recorded for the PGEO5MA$_{64}$ precursor prepared via RAFT aqueous solution polymerization of GEO5MA (black curve), the aldehyde-functional PAGEO5MA$_{64}$ homopolymer prepared via selective oxidation of this PGEO5MA$_{64}$ precursor (purple curve), and the PArgGEO5MA$_{64}$ homopolymer obtained via reductive amination after the Schiff base reaction of PAGEO5MA$_{64}$ with arginine at pH 10 (green trace). Apparent M_n values are expressed relative to a series of near-monodisperse poly(ethylene oxide) calibration standards.

Synthesis and Characterization of Arginine-Functionalized Diblock Copolymer Nanoparticles. Chain extension of this water-soluble dithiobenzoate-capped PGEO5MA$_{64}$ precursor via RAFT aqueous emulsion polymerization of benzyl methacrylate (BzMA) at 70 °C produced a series of PGEO5MA$_{64}$−PBzMA$_x$ nanoparticles. DMF GPC studies confirmed efficient chain extension and a relatively narrow molecular weight distribution in each case (Figure S1). Systematic variation of the target DP for the core-forming PBzMA$_x$ block from 50 to 500 produced six aqueous nanoparticle dispersions, with DLS studies indicating *z*-average diameters ranging from 31 to 61 nm (Figure 4a). A plot of such data reveals a monotonic increase in nanoparticle diameter (Figure S4). Similarly, the corresponding TEM images suggest a monotonic increase in the number-average diameter of the nanoparticle cores, D_n, in accordance with prior aqueous PISA formulations (Figure 4b−g).[59,70,71] In addition, the mean aggregation number, N_{agg}, or average number of copolymer chains per nanoparticle, was estimated for the smallest and largest nanoparticles. More specifically, the PBzMA core volume, V, was calculated from D_n using $V = \frac{1}{6}\pi D_n^3$. Hence the corresponding PBzMA core mass, m, is calculated using $m = \rho \cdot V$, where the density of PBzMA, ρ, is 1.15 g cm^{-3}; dividing m by the molar mass of the PBzMA$_x$ chains gives the mean aggregation number N_{agg}. Hence PGEO5MA$_{64}$−PBzMA$_{50}$ nanoparticles have an N_{agg} of 113, while the PGEO5MA$_{64}$−PBzMA$_{500}$ nanoparticles have an N_{agg} of 177.

The largest PGEO5MA$_{64}$−PBzMA$_{500}$ nanoparticles were selected for subsequent derivatization to aid their visualization after adsorption. Accordingly, $NaIO_4$ oxidation yielded the corresponding aldehyde-functional PAGEO5MA$_{64}$−PBzMA$_{500}$ nanoparticles, which were subsequently derivatized with arginine via reductive amination at pH 10 to yield cationic PArgGEO5MA$_{64}$−PBzMA$_{500}$ nanoparticles. DLS and TEM

https://doi.org/10.1021/acs.biomac.4c00128
Biomacromolecules 2024, 25, 2990−3000

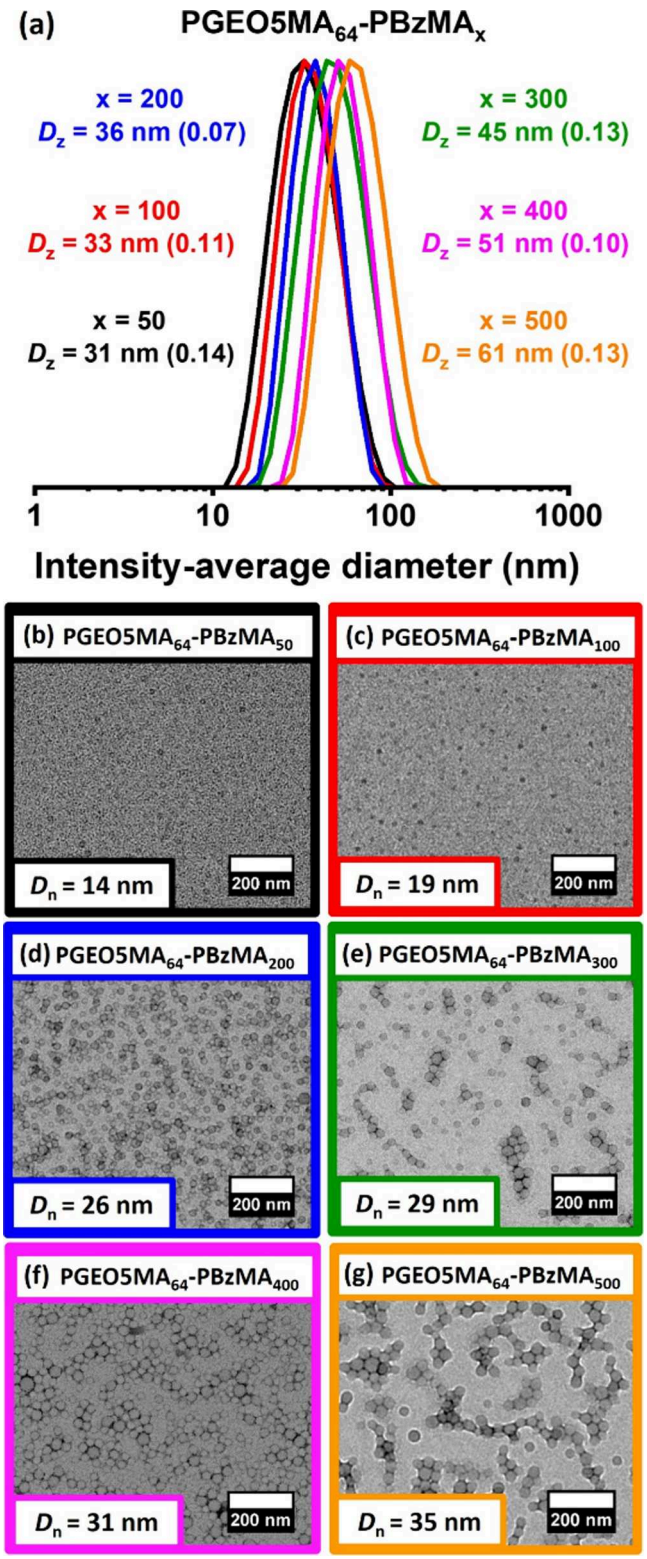

Figure 4. Particle size control by systematic variation of target PBzMA DP. (a) DLS particle size distributions (including *z*-average diameters and DLS polydispersities) and (b–g) corresponding TEM images recorded for a series of six examples of $PGEO5MA_{64}$–$PBzMA_x$ nanoparticles prepared via RAFT aqueous emulsion polymerization of benzyl methacrylate at 70 °C when targeting a PBzMA DP of 50–500.

studies of the corresponding nanoparticles confirmed that their morphology was not adversely affected during each derivatization (see Figure 5).

Aqueous electrophoresis was employed to assess the change in electrophoretic behavior of these nanoparticles during their derivatization. Accordingly, zeta potential versus pH curves were constructed from pH 2 to 10. As expected, the *cis*-diol-functionalized $PGEO5MA_{64}$–$PBzMA_{500}$ precursor nanoparticles and the aldehyde-functional $PGEO5MA_{64}$–$PBzMA_{500}$ nanoparticles remained essentially neutral across the whole pH range (see Figure 6a and 6b, respectively). In contrast, the $PArgGEO5MA_{64}$–$PBzMA_{500}$ nanoparticles exhibit significant cationic character. A zeta potential of around +34 mV is observed at pH 2, which corresponds to the regime in which the pendent primary amine and guanidine groups are both protonated, and the pendent carboxylic acid group is in its neutral (non-ionized) form. A gradual reduction to a plateau value of +22 mV occurs on raising the pH to 4.3, which then remains constant up to pH 7.2. In this second regime, the carboxylic acid group becomes ionized, which lowers the overall cationic surface charge. A further gradual reduction in zeta potential occurs thereafter owing to deprotonation of the pendent primary amine group, with essentially neutral character observed for these nanoparticles at around pH 10 (Figure 6c). Essentially the same zeta potential versus pH curve was obtained for the smaller $PArgGEO5MA_{64}$–$PBzMA_{50}$ nanoparticles (Figure S5).

Adsorption Studies of Arginine-Functionalized Diblock Copolymer Nanoparticles. Adsorption of the cationic $PArgGEO5MA_{64}$–$PBzMA_{500}$ nanoparticles onto a model planar substrate (silica) was studied at pH 7 using a QCM (Figure 7a). In such experiments, adsorbed nanoparticles are considered to form a rigid thin film so the Sauerbrey equation is valid. Strong nanoparticle adsorption (Γ = 14.7 mg m^{-2}; red curve) is observed at 25 °C. The silica surface is highly anionic at pH 7, which leads to electrostatic adsorption of the cationic nanoparticles. In contrast, despite their greater cationic character (see Figure 6c), nanoparticle adsorption is substantially reduced at pH 3 (Γ = 1.9 mg m^{-2}; orange curve). This is because the silica substrate exhibits almost no surface charge under these conditions so nanoparticle adsorption involves only van der Waals interactions. In a control experiment, the neutral $PGEO5MA_{64}$–$PBzMA_{500}$ precursor nanoparticles were also adsorbed onto silica at pH 7. In this case, similarly weak adsorption (Γ = 2.3 mg m^{-2}; black curve) was observed, again owing to the absence of any electrostatic attractive interactions. In both cases, the silica sensor was rinsed with deionized water immediately after nanoparticle adsorption, but no discernible change in frequency was observed.

SEM images were recorded for the QCM sensors after performing adsorption experiments using $PArgGEO5MA_{64}$–$PBzMA_{500}$ nanoparticles (Figure 7b). Using digital image analysis (*ImageJ* software), a surface coverage of 42% was calculated for electrostatic adsorption at pH 7 but just 5% surface coverage was estimated for the same nanoparticles adsorbed at pH 3. In summary, these experiments confirm that the extent of adsorption of arginine-functionalized $PArgGEO5MA_{64}$–$PBzMA_{500}$ nanoparticles onto silica is strongly pH-dependent.

Finally, QCM was used to study the adsorption of the smallest [DLS diameter = 31 nm (0.14)] $PArgGEO5MA_{64}$–$PBzMA_{50}$ nanoparticles at pH 7 (Figure 8). As expected, an

https://doi.org/10.1021/acs.biomac.4c00128
Biomacromolecules 2024, 25, 2990–3000

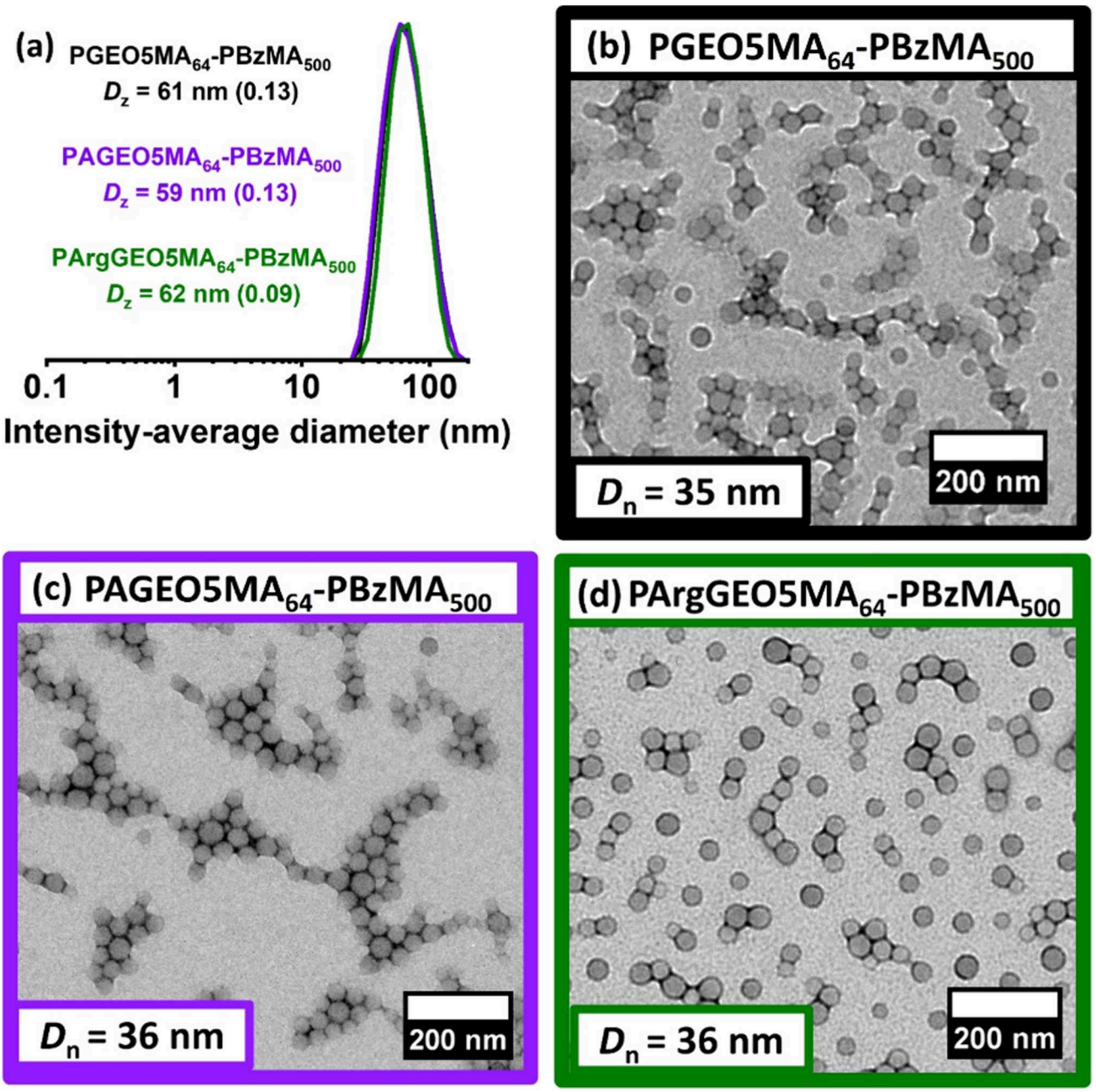

Figure 5. Effect of chemical functionality of the steric stabilizer chains on particle size. (a) DLS particle size distributions (including *z*-average diameters and DLS polydispersities) and corresponding TEM images recorded for (b) *cis*-diol-functionalized PGEO5MA$_{64}$−PBzMA$_{500}$ nanoparticles, (c) aldehyde-functionalized PAGEO5MA$_{64}$−PBzMA$_{500}$ nanoparticles, and (d) arginine-functionalized PArgGEO5MA$_{64}$−PBzMA$_{500}$ nanoparticles.

appreciably lower adsorbed amount (Γ = 10.6 mg m^{-2}) was observed compared to that obtained for the 61 nm DLS diameter PArgGEO5MA$_{64}$−PBzMA$_{500}$ nanoparticles (compare green and red curves). Brotherton et al. reported similar observations for the adsorption of sterically stabilized nanoparticles onto stainless steel from aqueous solution.[59] Moreover, the relatively small PArgGEO5MA$_{64}$−PBzMA$_{50}$ nanoparticles are clearly less strongly adsorbed at the silica surface because a minor fraction (8%) could be removed when rinsing with deionized water. In contrast, no reduction in the adsorbed amount occurs for the larger PArgGEO5MA$_{64}$−PBzMA$_{500}$ nanoparticles. Similar observations were made for the neutral PGEO5MA$_{64}$−PBzMA$_{50}$ and PGEO5MA$_{64}$−PBzMA$_{500}$ nanoparticles: a substantial proportion (68%) of the former could be removed by rinsing, whereas the adsorbed amount obtained for the latter remained essentially unchanged after rinsing (compare blue and black curves). Thus smaller nanoparticles adhere more weakly than larger nanoparticles in the absence of a strong electrostatic attractive interaction between the nanoparticles and the planar substrate. Conversely, introducing such an electrostatic interaction can minimize the partial loss of relatively small nanoparticles during rinsing. In summary, this is an interesting new model system for understanding the effect of particle size and electrostatic attractive forces on the (ir)reversible adsorption of electrosterically stabilized nanoparticles onto oppositely charged planar surfaces.

https://doi.org/10.1021/acs.biomac.4c00128
Biomacromolecules 2024, 25, 2990−3000

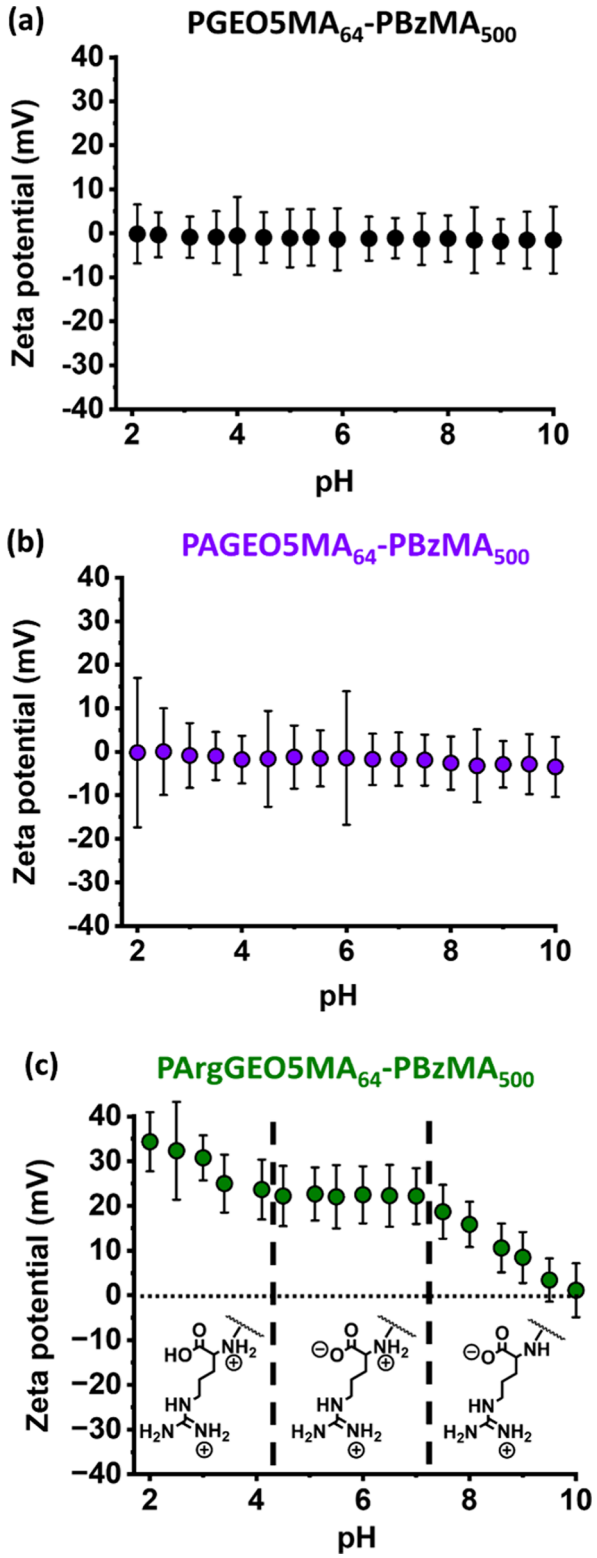

Figure 6. Aqueous electrophoresis data. Zeta potential versus pH curves obtained in the presence of 1 mM KCl for: (a) *cis*-diol-functionalized PGEO5MA$_{64}$−PBzMA$_{500}$ nanoparticles; (b) aldehyde-functionalized PAGEO5MA$_{64}$−PBzMA$_{500}$ nanoparticles; (c) arginine-functionalized PArgGEO5MA$_{64}$−PBzMA$_{500}$ nanoparticles. The two vertical dashed lines at pH 4.2 and pH 7.2 correspond to the approximate pK_a values for the deprotonation of the carboxylic acid and the primary amine of the pendent amino acid group in PArgGEO5MA$_{64}$, respectively.

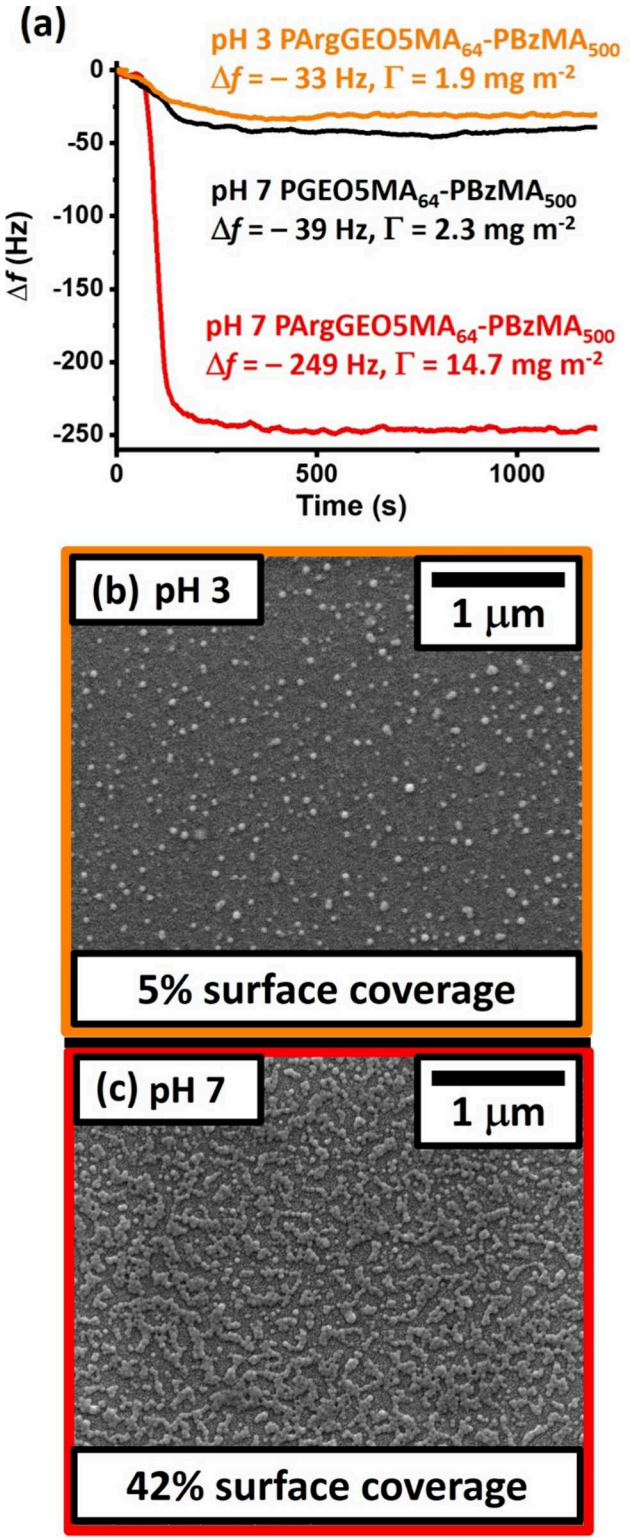

Figure 7. Effect of solution pH and chemical functionality on nanoparticle adsorption at a planar silica substrate. (a) QCM curves recorded during adsorption of neutral *cis*-diol-functionalized PGEO5MA$_{64}$−PBzMA$_{500}$ nanoparticles at pH 7 (black trace); cationic arginine-functionalized PArgGEO5MA$_{64}$−PBzMA$_{500}$ nanoparticles at pH 7 (red trace); and cationic arginine-functionalized PArgGEO5MA$_{64}$−PBzMA$_{500}$ nanoparticles at pH 3 (orange trace). Corresponding SEM images were recorded for arginine-functionalized PArgGEO5MA$_{64}$−PBzMA$_{500}$ nanoparticles adsorbed on the same silica surface at either (b) pH 3 or (c) pH 7. Digital image analysis (*ImageJ* software) indicated surface coverages of 5 and 42%, respectively.

https://doi.org/10.1021/acs.biomac.4c00128
Biomacromolecules 2024, 25, 2990−3000

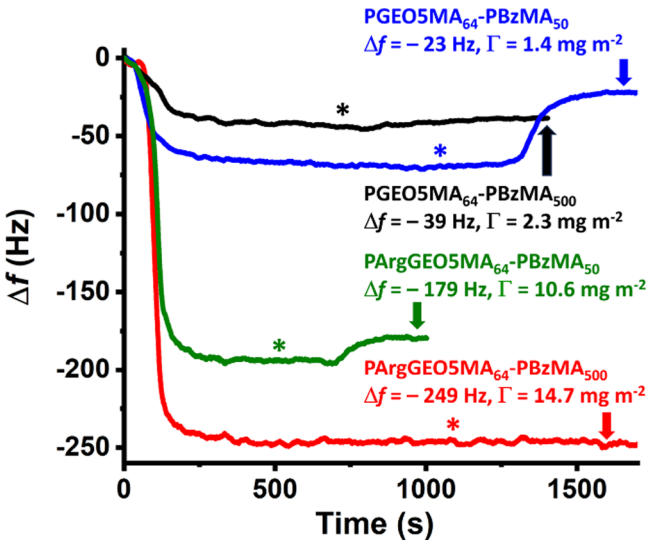

Figure 8. Effect of particle size and chemical functionality on nanoparticle adsorption at a planar silica substrate. QCM curves recorded at pH 7 during adsorption of the smallest (DLS diameter = 31 nm, blue trace) and largest (DLS diameter = 61 nm, black trace) *cis*-diol-functionalized PGEO5MA$_{64}$–PBzMA$_x$ nanoparticles and the corresponding cationic arginine-functionalized PArgGEO5MA$_{64}$–PBzMA$_x$ nanoparticles (red and green traces, respectively). The four asterisks indicate the points at which deionized water was introduced to remove any weakly adhering nanoparticles.

CONCLUSIONS

We demonstrate that a hydrophilic aldehyde-functional methacrylic polymer can be reacted with arginine in aqueous solution under mild conditions to produce the analogous arginine-functional methacrylic polymer. Importantly, this chemical derivatization can be achieved without recourse to protecting group chemistry. Careful control of the solution pH is essential to ensure regioselectivity for initial imine bond formation; subsequent reductive amination using $NaCNBH_3$ leads to a hydrolytically stable amide linkage. This protocol was then utilized to prepare arginine-functionalized diblock copolymer nanoparticles in aqueous media via PISA. Such functionalization did not adversely affect either the nanoparticle size distribution or the molecular weight distribution of the derivatized diblock copolymer chains. Aqueous electrophoresis studies confirmed that these arginine-functionalized nanoparticles exhibit cationic character between pH 2 and 9. A QCM instrument was used to study the adsorption of the resulting cationic nanoparticles onto a planar silica surface. Favorable electrostatic interactions led to strong adsorption at pH 7 (Γ = 14.7 mg m^{-2}). In contrast, much weaker adsorption was observed at pH 3 (Γ = 1.9 mg m^{-2}) because the silica substrate has almost no anionic surface charge under such conditions. These findings were corroborated by SEM studies, which indicated surface coverages of 42% at pH 7 and 5% at pH 3, respectively. Finally, minimal nanoparticle adsorption was also observed at pH 10 because the nanoparticles are close to their isoelectric point under such conditions.

ASSOCIATED CONTENT

Supporting Information

The Supporting Information is available free of charge at https://pubs.acs.org/doi/10.1021/acs.biomac.4c00128.

DMF GPC curves recorded for the PGEO5MA$_{64}$ precursor and PGEO5MA$_{64}$–PBzMA$_x$ diblock copolymers; ^{1}H NMR spectrum recorded for PGEO5MA$_{64}$–PBzMA$_{500}$ diblock copolymer; and ^{1}H NMR spectrum recorded for PAGEO5MA$_{64}$–PBzMA$_{500}$ diblock copolymer (PDF)

AUTHOR INFORMATION

Corresponding Author

Steven P. Armes − *Dainton Building, Department of Chemistry, University of Sheffield, Sheffield, South Yorkshire S3 7HF, U.K.*; orcid.org/0000-0002-8289-6351; Email: s.p.armes@shef.ac.uk

Authors

Hubert Buksa − *Dainton Building, Department of Chemistry, University of Sheffield, Sheffield, South Yorkshire S3 7HF, U.K.*

Edwin C. Johnson − *Dainton Building, Department of Chemistry, University of Sheffield, Sheffield, South Yorkshire S3 7HF, U.K.*; orcid.org/0000-0002-0092-1008

Derek H. H. Chan − *Dainton Building, Department of Chemistry, University of Sheffield, Sheffield, South Yorkshire S3 7HF, U.K.*

Rory J. McBride − *Dainton Building, Department of Chemistry, University of Sheffield, Sheffield, South Yorkshire S3 7HF, U.K.*; orcid.org/0009-0003-4611-9293

George Sanderson − *GEO Specialty Chemicals, Hythe, Southampton, Hampshire SO45 3ZG, U.K.*

Rebecca M. Corrigan − *School of Biosciences and The Florey Institute for Host–Pathogen Interactions, University of Sheffield, Sheffield, South Yorkshire S10 2TN, U.K.*

Complete contact information is available at: https://pubs.acs.org/10.1021/acs.biomac.4c00128

Notes

The authors declare no competing financial interest.

ACKNOWLEDGMENTS

We thank EPSRC for a CASE PhD studentship for the first author and thank GEO Specialty Chemicals for additional financial support of this project and for permission to publish these results. We also acknowledge an EPSRC Programme Grant (EP/T012455/1) for postdoctoral support of E.C.J. R.M.C. thanks the Wellcome Trust and the Royal Society (104110/Z/14/A) for a Sir Henry Dale Fellowship and acknowledges a 2018 Lister Institute Research Prize. We thank Christopher Hill and Dr. Svetomir Tzokov of the University of Sheffield Biomedical Science Electron Microscopy suite for their technical assistance. Finally, Dr. Raffaele Battaglia and Marco Mauro at Novaetech S.r.l. (Pompeii, Italy) are thanked for their excellent technical support regarding the QCM-D studies.

REFERENCES

(1) Luo, K.; Li, C.; Li, L.; She, W.; Wang, G.; Gu, Z. Arginine Functionalized Peptide Dendrimers as Potential Gene Delivery Vehicles. *Biomaterials* **2012**, *33*, 4917–4927.

(2) Ma, D.; Lin, Q. M.; Zhang, L. M.; Liang, Y. Y.; Xue, W. A Star-Shaped Porphyrin-Arginine Functionalized Poly(*L*-Lysine) Copolymer for Photo-Enhanced Drug and Gene Co-Delivery. *Biomaterials* **2014**, *35*, 4357–4367.

(3) Memanishvili, T.; Zavradashvili, N.; Kupatadze, N.; Tugushi, D.; Gverdtsiteli, M.; Torchilin, V. P.; Wandrey, C.; Baldi, L.; Manoli, S. S.; Katsarava, R. Arginine-Based Biodegradable Ether−Ester Polymers with Low Cytotoxicity as Potential Gene Carriers. *Biomacromolecules* **2014**, *15*, 2839−2848.
(4) Xu, G.; Liu, X.; Liu, P.; Pranantyo, D.; Neoh, K.-G.; Kang, E.-T. Arginine-Based Polymer Brush Coatings with Hydrolysis-Triggered Switchable Functionalities from Antimicrobial (Cationic) to Antifouling (Zwitterionic). *Langmuir* **2017**, *33*, 6925−6936.
(5) Ferruti, P.; Mauro, N.; Falciola, L.; Pifferi, V.; Bartoli, C.; Gazzarri, M.; Chiellini, F.; Ranucci, E. Amphoteric, Prevailingly Cationic *L*-Arginine Polymers of Poly(Amidoamino Acid) Structure: Synthesis, Acid/Base Properties and Preliminary Cytocompatibility and Cell-Permeating Characterizations. *Macromol. Biosci.* **2014**, *14*, 390−400.
(6) Zavradashvili, N.; Sarisozen, C.; Titvinidze, G.; Otinashvili, G.; Kantaria, T.; Tugushi, D.; Puiggali, J.; Torchilin, V. P.; Katsarava, R. Library of Cationic Polymers Composed of Polyamines and Arginine as Gene Transfection Agents. *ACS Omega* **2019**, *4*, 2090−2101.
(7) Heydari, P.; Varshosaz, J.; Kharaziha, M.; Javanmard, S. H. Antibacterial and pH-Sensitive Methacrylate Poly-*L*-Arginine/Poly (*β*-Amino Ester) Polymer for Soft Tissue Engineering. *J. Mater. Sci. Mater. Med.* **2023**, *34*, 34.
(8) De Oliveira, D. M. P.; Forde, B. M.; Kidd, T. J.; Harris, P. N. A.; Beatson, S. A.; Paterson, D. L.; Walker, J. Antimicrobial Resistance in ESKAPE Pathogens. *Clin. Microbiol. Rev.* **2020**, *33*, No. e00181-19.
(9) Kuroki, A.; Kengmo Tchoupa, A.; Hartlieb, M.; Peltier, R.; Locock, K. E. S.; Unnikrishnan, M.; Perrier, S. Targeting Intracellular, Multi-Drug Resistant *Staphylococcus Aureus* with Guanidinium Polymers by Elucidating the Structure-Activity Relationship. *Biomaterials* **2019**, *217*, No. 119249.
(10) Zhao, Q.; Liu, Q.; Li, C.; Cao, L.; Ma, L.; Wang, X.; Cai, Y. Noncovalent Structural Locking of Thermoresponsive Polyion Complex Micelles, Nanowires, and Vesicles via Polymerization-Induced Electrostatic Self-Assembly Using an Arginine-like Monomer. *Chem. Commun.* **2020**, *56*, 4954−4957.
(11) Jackson, A. W.; Fulton, D. A. The Formation of Core Cross-Linked Star Polymers Containing Cores Cross-Linked by Dynamic Covalent Imine Bonds. *Chem. Commun.* **2010**, *46*, 6051−6053.
(12) Murray, B. S.; Jackson, A. W.; Mahon, C. S.; Fulton, D. A. Reactive Thermoresponsive Copolymer Scaffolds. *Chem. Commun.* **2010**, *46*, 8651−8653.
(13) Ferguson, C. J.; Hughes, R. J.; Pham, B. T. T.; Hawkett, B. S.; Gilbert, R. G.; Serelis, A. K.; Such, C. H. Effective Ab Initio Emulsion Polymerization under RAFT Control. *Macromolecules* **2002**, *35*, 9243−9245.
(14) Ferguson, C.; Hughes, R.; Nguyen, D.; Pham, B.; Gilbert, R.; Serelis, A.; Such, C.; Hawkett, B. Ab Initio Emulsion Polymerization by RAFT-Controlled Self-Assembly. *Macromolecules* **2005**, *38*, 2191−2204.
(15) Wan, W. M.; Sun, X. L.; Pan, C. Y. Morphology Transition in RAFT Polymerization for Formation of Vesicular Morphologies in One Pot. *Macromolecules* **2009**, *42*, 4950−4952.
(16) Wan, W. M.; Pan, C. Y. One-Pot Synthesis of Polymeric Nanomaterials via RAFT Dispersion Polymerization Induced Self-Assembly and Re-Organization. *Polym. Chem.* **2010**, *1*, 1475−1484.
(17) Cai, W.; Wan, W.; Hong, C.; Huang, C.; Pan, C. Morphology Transitions in RAFT Polymerization. *Soft Matter* **2010**, *6*, 5554−5561.
(18) He, W.-D.; Sun, X.-L.; Wan, W.-M.; Pan, C.-Y. Multiple Morphologies of PAA-b-PSt Assemblies throughout RAFT Dispersion Polymerization of Styrene with PAA Macro-CTA. *Macromolecules* **2011**, *44*, 3358−3365.
(19) Rieger, J.; Stoffelbach, F.; Bui, C.; Alaimo, D.; Jérôme, C.; Charleux, B. Amphiphilic Poly(Ethylene Oxide) Macromolecular RAFT Agent as a Stabilizer and Control Agent in Ab Initio Batch Emulsion Polymerization. *Macromolecules* **2008**, *41*, 4065−4068.
(20) Zhang, X.; Boissé, S.; Zhang, W.; Beaunier, P.; D'Agosto, F.; Rieger, J.; Charleux, B. Well-Defined Amphiphilic Block Copolymers and Nano-Objects Formed in Situ via RAFT-Mediated Aqueous Emulsion Polymerization. *Macromolecules* **2011**, *44*, 4149−4158.
(21) Rieger, J.; Osterwinter, G.; Bui, C.; Stoffelbnach, F.; Charleux, B. Surfactant-Free Controlled/Living Radical Emulsion (Co)-Polymerization of n-Butyl Acrylate and Methyl Methacrylate via RAFT Using Amphiphilic Polyethylene Oxide-Based Trithiocarbonate Chain Transfer Agents. *Macromolecules* **2009**, *42*, 5518−5525.
(22) Chaduc, I.; Lansalot, M.; D'Agosto, F.; Charleux, B. RAFT Polymerization of Methacrylic Acid in Water. *Macromolecules* **2012**, *45*, 1241−1247.
(23) Charleux, B.; Delaittre, G.; Rieger, J.; D'Agosto, F. Polymerization-Induced Self-Assembly: From Soluble Macromolecules to Block Copolymer Nano-Objects in One Step. *Macromolecules* **2012**, *45*, 6753−6765.
(24) Chaduc, I.; Girod, M.; Antoine, R.; Charleux, B.; D'Agosto, F.; Lansalot, M. Batch Emulsion Polymerization Mediated by Poly-(Methacrylic Acid) MacroRAFT Agents: One-Pot Synthesis of Self-Stabilized Particles. *Macromolecules* **2012**, *45*, 5881−5893.
(25) Zhang, X.; Rieger, J.; Charleux, B. Effect of the Solvent Composition on the Morphology of Nano-Objects Synthesized via RAFT Polymerization of Benzyl Methacrylate in Dispersed Systems. *Polym. Chem.* **2012**, *3*, 1502−1509.
(26) An, Z.; Shi, Q.; Tang, W.; Tsung, C. K.; Hawker, C. J.; Stucky, G. D. Facile RAFT Precipitation Polymerization for the Microwave-Assisted Synthesis of Well-Defined, Double Hydrophilic Block Copolymers and Nanostructured Hydrogels. *J. Am. Chem. Soc.* **2007**, *129*, 14493−14499.
(27) Zetterlund, P. B.; Thickett, S. C.; Perrier, S.; Bourgeat-Lami, E.; Lansalot, M. Controlled/Living Radical Polymerization in Dispersed Systems: An Update. *Chem. Rev.* **2015**, *115*, 9745−9800.
(28) D'Agosto, F.; Rieger, J.; Lansalot, M. RAFT-Mediated Polymerization-Induced Self-Assembly. *Angew. Chemie - Int. Ed.* **2020**, *59*, 8368−8392.
(29) Canning, S. L.; Smith, G. N.; Armes, S. P. A Critical Appraisal of RAFT-Mediated Polymerization-Induced Self-Assembly. *Macromolecules* **2016**, *49*, 1985−2001.
(30) Warren, N. J.; Armes, S. P. Polymerization-Induced Self-Assembly of Block Copolymer Nano-Objects via RAFT Aqueous Dispersion Polymerization. *J. Am. Chem. Soc.* **2014**, *136*, 10174−10185.
(31) Mellot, G.; Guigner, J. M.; Bouteiller, L.; Stoffelbach, F.; Rieger, J. Templated PISA: Driving Polymerization-Induced Self-Assembly towards Fibre Morphology. *Angew. Chemie - Int. Ed.* **2019**, *58*, 3173−3177.
(32) Debrie, C.; Coudert, N.; Guigner, J. M.; Nicolai, T.; Stoffelbach, F.; Colombani, O.; Rieger, J. Unimer Exchange Is Not Necessary for Morphological Transitions in Polymerization-Induced Self-Assembly. *Angew. Chemie - Int. Ed.* **2023**, *62*, 1−6.
(33) Clothier, G. K. K.; Guimarães, T. R.; Khan, M.; Moad, G.; Perrier, S.; Zetterlund, P. B. Exploitation of the Nanoreactor Concept for Efficient Synthesis of Multiblock Copolymers via Macroraft-Mediated Emulsion Polymerization. *ACS Macro Lett.* **2019**, *8*, 989−995.
(34) Guimarães, T. R.; Khan, M.; Kuchel, R. P.; Morrow, I. C.; Minami, H.; Moad, G.; Perrier, S.; Zetterlund, P. B. Nano-Engineered Multiblock Copolymer Nanoparticles via Reversible Addition-Fragmentation Chain Transfer Emulsion Polymerization. *Macromolecules* **2019**, *52*, 2965−2974.
(35) Khan, M.; Guimarães, T. R.; Kuchel, R. P.; Moad, G.; Perrier, S.; Zetterlund, P. B. Synthesis of Multicompositional Onion-like Nanoparticles via RAFT Emulsion Polymerization. *Angew. Chemie - Int. Ed.* **2021**, *60*, 23281−23288.
(36) Shen, W.; Chang, Y.; Liu, G.; Wang, H.; Cao, A.; An, Z. Biocompatible, Antifouling, and Thermosensitive Core-Shell Nanogels Synthesized by RAFT Aqueous Dispersion Polymerization. *Macromolecules* **2011**, *44*, 2524−2530.
(37) Liu, G.; Qiu, Q.; Shen, W.; An, Z. Aqueous Dispersion Polymerization of 2-Methoxyethyl Acrylate for the Synthesis of

https://doi.org/10.1021/acs.biomac.4c00128
Biomacromolecules 2024, 25, 2990−3000

Biocompatible Nanoparticles Using a Hydrophilic RAFT Polymer and a Redox Initiator. *Macromolecules* **2011**, *44*, 5237−5245.
(38) Tan, J.; Liu, D.; Bai, Y.; Huang, C.; Li, X.; He, J.; Xu, Q.; Zhang, L. Enzyme-Assisted Photoinitiated Polymerization-Induced Self-Assembly: An Oxygen-Tolerant Method for Preparing Block Copolymer Nano-Objects in Open Vessels and Multiwell Plates. *Macromolecules* **2017**, *50*, 5798−5806.
(39) Dai, X.; Yu, L.; Zhang, Y.; Zhang, L.; Tan, J. Polymerization-Induced Self-Assembly via RAFT-Mediated Emulsion Polymerization of Methacrylic Monomers. *Macromolecules* **2019**, *52*, 7468−7476.
(40) Zhang, Q.; Zeng, R.; Zhang, Y.; Chen, Y.; Zhang, L.; Tan, J. Two Polymersome Evolution Pathways in One Polymerization-Induced Self-Assembly (PISA) System. *Macromolecules* **2020**, *53*, 8982−8991.
(41) Xiong, W.; Wang, X.; Liu, Y.; Luo, C.; Lu, X.; Cai, Y. Polymerization-Induced Electrostatic Self-Assembly Governed by Guanidinium Ionic Hydrogen Bonds. *Macromolecules* **2022**, *55*, 7003−7012.
(42) Figg, C. A.; Simula, A.; Gebre, K. A.; Tucker, B. S.; Haddleton, D. M.; Sumerlin, B. S. Polymerization-Induced Thermal Self-Assembly (PITSA). *Chem. Sci.* **2015**, *6*, 1230−1236.
(43) Tan, J.; Sun, H.; Yu, M.; Sumerlin, B. S.; Zhang, L. Photo-PISA: Shedding Light on Polymerization-Induced Self-Assembly. *ACS Macro Lett.* **2015**, *4*, 1249−1253.
(44) Blackman, L. D.; Varlas, S.; Arno, M. C.; Houston, Z. H.; Fletcher, N. L.; Thurecht, K. J.; Hasan, M.; Gibson, M. I.; O'Reilly, R. K. Confinement of Therapeutic Enzymes in Selectively Permeable Polymer Vesicles by Polymerization-Induced Self-Assembly (PISA) Reduces Antibody Binding and Proteolytic Susceptibility. *ACS Cent. Sci.* **2018**, *4*, 718−723.
(45) Blackman, L. D.; Doncom, K. E. B.; Gibson, M. I.; O'Reilly, R. K. Comparison of Photo- and Thermally Initiated Polymerization-Induced Self-Assembly: A Lack of End Group Fidelity Drives the Formation of Higher Order Morphologies. *Polym. Chem.* **2017**, *8*, 2860−2871.
(46) Blanazs, A.; Madsen, J.; Battaglia, G.; Ryan, A. J.; Armes, S. P. Mechanistic Insights for Block Copolymer Morphologies: How Do Worms Form Vesicles? *J. Am. Chem. Soc.* **2011**, *133*, 16581−16587.
(47) Blanazs, A.; Verber, R.; Mykhaylyk, O. O.; Ryan, A. J.; Heath, J. Z.; Douglas, C. W. I.; Armes, S. P. Sterilizable Gels from Thermoresponsive Block Copolymer Worms. *J. Am. Chem. Soc.* **2012**, *134*, 9741−9748.
(48) Chambon, P.; Blanazs, A.; Battaglia, G.; Armes, S. Facile Synthesis of Methacrylic ABC Triblock Copolymer Vesicles by RAFT Aqueous Dispersion Polymerization. *Macromolecules* **2012**, *45*, 5081−5090.
(49) Yang, P.; Mykhaylyk, O. O.; Jones, E. R.; Armes, S. P. RAFT Dispersion Alternating Copolymerization of Styrene with N-Phenylmaleimide: Morphology Control and Application as an Aqueous Foam Stabilizer. *Macromolecules* **2016**, *49*, 6731−6742.
(50) Yang, P.; Ratcliffe, L. P. D.; Armes, S. P. Efficient Synthesis of Poly(Methacrylic Acid)-Block-Poly(Styrene-Alt-N-Phenylmaleimide) Diblock Copolymer Lamellae Using RAFT Dispersion Polymerization. *Macromolecules* **2013**, *46*, 8545−8556.
(51) Albigès, R.; Klein, P.; Roi, S.; Stoffelbach, F.; Creton, C.; Bouteiller, L.; Rieger, J. Water-Based Acrylic Coatings Reinforced by PISA-Derived Fibers. *Polym. Chem.* **2017**, *8*, 4992−4995.
(52) Derry, M. J.; Smith, T.; O'Hora, P. S.; Armes, S. P. Block Copolymer Nanoparticles Prepared via Polymerization-Induced Self-Assembly Provide Excellent Boundary Lubrication Performance for Next-Generation Ultralow-Viscosity Automotive Engine Oils. *ACS Appl. Mater. Interfaces* **2019**, *11*, 33364−33369.
(53) Hunter, S. J.; Armes, S. P. Pickering Emulsifiers Based on Block Copolymer Nanoparticles Prepared by Polymerization-Induced Self-Assembly. *Langmuir* **2020**, *36*, 15463−15484.
(54) György, C.; Kirkman, P. M.; Neal, T. J.; Chan, D. H. H.; Williams, M.; Smith, T.; Growney, D. J.; Armes, S. P. Enhanced Adsorption of Epoxy-Functional Nanoparticles onto Stainless Steel Significantly Reduces Friction in Tribological Studies. *Angew. Chemie - Int. Ed.* **2023**, *62*, No. e202218397.
(55) Canton, I.; Warren, N. J.; Chahal, A.; Amps, K.; Wood, A.; Weightman, R.; Wang, E.; Moore, H.; Armes, S. P. Mucin-Inspired Thermoresponsive Synthetic Hydrogels Induce Stasis in Human Pluripotent Stem Cells and Human Embryos. *ACS Cent. Sci.* **2016**, *2*, 65−74.
(56) Inam, M.; Jones, J. R.; Pérez-Madrigal, M. M.; Arno, M. C.; Dove, A. P.; O'Reilly, R. K. Controlling the Size of Two-Dimensional Polymer Platelets for Water-in-Water Emulsifiers. *ACS Cent. Sci.* **2018**, *4*, 63−70.
(57) Brotherton, E. E.; Jesson, C. P.; Warren, N. J.; Smallridge, M. J.; Armes, S. P. New Aldehyde-Functional Methacrylic Water-Soluble Polymers. *Angew. Chemie - Int. Ed.* **2021**, *133*, 12139−12144.
(58) Brotherton, E. E.; Smallridge, M. J.; Armes, S. P. Aldehyde-Functional Diblock Copolymer Nano-Objects via RAFT Aqueous Dispersion Polymerization. *Biomacromolecules* **2021**, *22*, 5382−5389.
(59) Brotherton, E. E.; Josland, D.; György, C.; Johnson, E. C.; Chan, D. H. H.; Smallridge, M. J.; Armes, S. P. Histidine-Functionalized Diblock Copolymer Nanoparticles Exhibit Enhanced Adsorption onto Planar Stainless Steel. *Macromol. Rapid Commun.* **2023**, *44*, 44.
(60) Brotherton, E. E.; Johnson, E. C.; Smallridge, M. J.; Hammond, D. B.; Leggett, G. J.; Armes, S. P. Hydrophilic Aldehyde-Functional Polymer Brushes: Synthesis, Characterization, and Potential Bioapplications. *Macromolecules* **2023**, *56*, 2070−2080.
(61) Matyjaszewski, K. Atom Transfer Radical Polymerization (ATRP): Current Status and Future Perspectives. *Macromolecules* **2012**, *45*, 4015−4039.
(62) Engström, J.; Reid, M. S.; Brotherton, E. E.; Malmström, E.; Armes, S. P.; Hatton, F. L. Investigating the Adsorption of Anisotropic Diblock Copolymer Worms onto Planar Silica and Nanocellulose Surfaces Using a Quartz Crystal Microbalance. *Polym. Chem.* **2021**, *12*, 6088−6100.
(63) Olsson, A. L. J.; Quevedo, I. R.; He, D.; Basnet, M.; Tufenkji, N. Using the Quartz Crystal Microbalance with Dissipation Monitoring to Evaluate the Size of Nanoparticles Deposited on Surfaces. *ACS Nano* **2013**, *7*, 7833−7843.
(64) Olsson, A. L. J.; Mitzel, M. R.; Tufenkji, N. QCM-D for Non-Destructive Real-Time Assessment of *Pseudomonas Aeruginosa* Biofilm Attachment to the Substratum during Biofilm Growth. *Colloids Surf. B. Biointerfaces* **2015**, *136*, 928−934.
(65) Fatisson, J.; Domingos, R. F.; Wilkinson, K. J.; Tufenkji, N. Deposition of TiO2 Nanoparticles onto Silica Measured Using a Quartz Crystal Microbalance with Dissipation Monitoring. *Langmuir* **2009**, *25*, 6062−6069.
(66) Easley, A. D.; Ma, T.; Eneh, C. I.; Yun, J.; Thakur, R. M.; Lutkenhaus, J. L. A Practical Guide to Quartz Crystal Microbalance with Dissipation Monitoring of Thin Polymer Films. *J. Polym. Sci.* **2022**, *60*, 1090−1107.
(67) Adamczyk, Z.; Sadowska, M.; Żeliszewska, P. Applicability of QCM-D for Quantitative Measurements of Nano- and Microparticle Deposition Kinetics: Theoretical Modeling and Experiments. *Anal. Chem.* **2020**, *92*, 15087−15095.
(68) Tellechea, E.; Johannsmann, D.; Steinmetz, N. F.; Richter, R. P.; Reviakine, I. Model-Independent Analysis of QCM Data on Colloidal Particle Adsorption. *Langmuir* **2009**, *25*, 5177−5184.
(69) Fitch, C. A.; Platzer, G.; Okon, M.; Garcia-Moreno, B. E.; McIntosh, L. P. Arginine: Its pKa Value Revisited. *Protein Sci.* **2015**, *24*, 752−761.
(70) Cunningham, V. J.; Alswieleh, A. M.; Thompson, K. L.; Williams, M.; Leggett, G. J.; Armes, S. P.; Musa, O. M. Poly(Glycerol Monomethacrylate)-Poly(Benzyl Methacrylate) Diblock Copolymer Nanoparticles via RAFT Emulsion Polymerization: Synthesis, Characterization, and Interfacial Activity. *Macromolecules* **2014**, *47*, 5613−5623.
(71) Hatton, F. L.; Lovett, J. R.; Armes, S. P. Synthesis of Well-Defined Epoxy-Functional Spherical Nanoparticles by RAFT Aqueous Emulsion Polymerization. *Polym. Chem.* **2017**, *8*, 4856−4868.

https://doi.org/10.1021/acs.biomac.4c00128
Biomacromolecules 2024, 25, 2990−3000